

# Characterization of ordered array of micropores in a polymer film

Lulu Song,<sup>†a</sup> Vivek Sharma,<sup>‡b</sup> Jung Ok Park<sup>cd</sup> and Mohan Srinivasarao<sup>\*cde</sup>

Received 11th July 2010, Accepted 26th October 2010

DOI: 10.1039/c0sm00664e

Microporous polymer films prepared by templating “breath figures” tend to have closely packed, hexagonal arrays of pores. We characterize the hexagonal order of the structured films using Fraunhofer diffraction patterns in reciprocal space, as well as with the use of Voronoi diagrams and bond-orientational correlation functions using real space images. The average spacing of the pores over a wider area can be calculated by two-dimensional Bragg equation, while the analysis of microscope images provides a direct measurement of the average open pore size and its distribution. The use of bond-orientational correlation function is particularly useful in quantifying the order of various films formed under various conditions. Further, we show how the sequential ordering of water drops formed during breath-figure-templated assembly process can also be characterized using Voronoi analysis and bond orientational correlation function.

## 1. Introduction

Microporous polymer films with hexagonally packed pores in a near uniform size can be prepared simply by casting dilute polymer solutions in volatile solvents in the presence of moist airflow.<sup>1–14</sup> It has been shown that the micropore array is the fossilized version<sup>2,13</sup> of “breath figures” formed over evaporatively cooled polymer solution.<sup>2–6,14</sup> Breath figures refer to the patterns formed by condensing water drops when moist air (breath) is blown over cold substrates; typically nucleation and growth of water drops occur under partial wetting conditions, and patterns formed over solid substrates contain random patterns of polydisperse size drops.<sup>15–21</sup> In contrast, the breath figures formed over evaporative polymer solutions contain highly ordered arrays of nearly monodisperse drops. While the mechanistic details of this breath-figure-templated assembly of pores are still being pursued vigorously,<sup>2–6</sup> it is clear that the nucleation and growth of water droplets occur due to cooling caused by solvent evaporation.<sup>14</sup> The growing drops eventually crystallize into ordered arrays, and then evaporate away to leave behind the fossilized array of pores on the polymer film. A similar array of pores is created when a dispersion of inorganic particles in organic volatile solvent is used.<sup>22,23</sup> In this paper, we primarily focus on the characterization of the hexagonal order of these structured films formed by using dilute polystyrene

solutions, where carbon disulfide was used as a solvent. We also provide a glimpse of breath-figure-assembly process, showing how degree of order can be studied and interpreted by using the techniques discussed for analyzing holey films.

The highly ordered microstructure and the simplicity of the preparation make the “holey” films formed by breath-figure-templated assembly potentially useful for many diverse applications including photonic band gap materials and heterojunction devices,<sup>9</sup> pico- to femto-litre beakers for small quantity analysis,<sup>10</sup> ceramic microstructures,<sup>24</sup> light emitting diodes,<sup>25,26</sup> cell culturing and tissue engineering,<sup>11,12</sup> protein micropatterning<sup>27</sup> and honeycomb carbon nanotubes,<sup>22,23</sup> to name a few. Many of these applications require films with known degree of order. The present study illustrates how this underlying order can be quantified by characterization methods both in the reciprocal space using diffraction as well as in the real space using Voronoi analysis and bond-orientational correlation functions.

Sommerfeld in his classic text on Optics<sup>28</sup> provides the example of breath figures as a pattern that can be used to illustrate the diffraction arising from many randomly distributed particles. Indeed it is quite fascinating that the application of diffraction analysis to ordered porous films formed by breath-figure-templated assembly included in this study provides the complementary example of diffraction from ordered structure.

The methodology demonstrated here is useful for determining the regularity and order in patterns and assemblies formed by diverse methods and materials. Examples of similar studies can be found in a variety of systems, such as colloidal crystals,<sup>29,30</sup> bubble rafts,<sup>31</sup> Coulomb crystal formed by plasma,<sup>32</sup> block copolymer assemblies,<sup>33</sup> patterns formed by Bernard–Marangoni convection,<sup>34–36</sup> etc. Moreover, these methods can also be used in the analysis of patterned surfaces formed by lithography as well by self-assembly in biological world and in industrial settings. We demonstrate how the real space analysis with Voronoi polygons and orientation-correlation functions can be used to quantify the emergence of order in close-packed arrays of water drops. The understanding of ordering during growth and assembly process will lead us to a better understanding of the

<sup>a</sup>Nalco Energy Service, Sugar Land, TX, USA

<sup>b</sup>Hatsopoulos Microfluids Laboratory, Mechanical Engineering, Massachusetts Institute of Technology, Cambridge, MA, USA

<sup>c</sup>School of Material Science and Engineering, Georgia Institute of Technology, Atlanta, GA, USA. E-mail: mohan@mse.gatech.edu; jung.park@mse.gatech.edu; Tel: +1 404-894-9348

<sup>d</sup>Center for Advanced Research on Optical Microscopy, Georgia Institute of Technology, Atlanta, GA, USA

<sup>e</sup>School of Chemistry and Biochemistry, Georgia Institute of Technology, Atlanta, GA, USA

<sup>†</sup> Current address: Nalco Energy Service, Sugar Land, TX, USA.

<sup>‡</sup> Current address: Hatsopoulos Microfluids Laboratory, Mechanical Engineering, Massachusetts Institute of Technology, Cambridge, MA, USA.

mechanism and eventually to a better control of the size dispersity and order in porous films.

## 2. Experimental

Two types of polymers were used in this study: atactic polystyrene (a-PS) and poly[*p*-(phenylene)ethynylene] (PPE) with hexoxy side chain (hexo-PPE). The flexible chain polymer, a-PS, has weight-average molecular weight of 50 000 and a carboxylic acid terminal group, and was purchased from Scientific Polymer Products. The semiconducting polymer, hexo-PPE, was obtained from Prof. U. Bunz at Georgia Institute of Technology (currently at the University of Heidelberg). Polymers were dissolved in a volatile organic solvent, carbon disulfide (Reagent A.C.S., Fisher Scientific).

After a drop ( $\sim 0.15 \text{ cm}^3$ ) of polystyrene solution with a typical concentration of 1 wt% is spread onto a clean microscope slide, the slide is immediately transferred into a humidity-controlled chamber and moist air is passed across the surface of the solution. The temperature and humidity of the airflow are monitored and well controlled in the chamber, while different airflow speeds can be realized. Carbon disulfide evaporates quickly, leaving behind an opaque yet iridescent polymer film sticking to the glass slide, generally within tens of seconds depending on the volume of the drop and the airflow rate. For imaging purpose, the microporous films were made in a glass chamber on a microscope stage.

An optical microscope (Leica DMRX, 40 $\times$ /NA 0.75 dry objective) coupled with a CCD camera is used to image the films and, with the help of a Bertrand lens, the corresponding Fraunhofer diffraction patterns. An interference filter (central  $\lambda = 532 \pm 2 \text{ nm}$ , FWHM =  $10 \pm 2 \text{ nm}$ ) was used to provide near monochromatic illumination. To obtain sharp diffraction patterns, the aperture diaphragm is closed down to a minimum to create a well-collimated, normal-incident light beam on the sample.

The stages of breath-figure-assembly process were captured by a high-speed digital camera (Photron FASTCAM-DVR) which was connected to an optical microscope (Leica DMLSP). A long-work-distance objective (50 $\times$ /NA 0.5 L) was used to record the film forming process in the transmission mode. The underlying polymer solution contained a polymer with rigid backbone: hexo-PPE dissolved in carbon disulfide. Images were captured at 125 frames per second, and all the observations were made at central region of the films. The coordinates of pores in macroporous films and water drops undergoing assembly process were computed using Image Pro, and these coordinates were then used for the Voronoi analysis as well as for calculating bond-orientational correlation using Matlab codes written for this purpose.

## 3. Characterization of hexagonal order

### 3.1. Reciprocal space analysis of holey films

**3.1.1. Image formation.** In an optical microscope, when well-collimated light is normally incident onto a sample in the transmitted mode, light will be transmitted in different directions with certain amplitude transmission function depending on the optical properties of the sample.<sup>37</sup> Light waves leaving the sample film in the propagation direction are focused by an objective to

a point in its back focal plane, where they are made to interfere. All of the focused points form a diffraction pattern in the back focal plane with the position of each point corresponding to a diffraction angle (angle between the diffracted beam and the incident beam). For Gaussian optics (*i.e.*, small angle or paraxial approximation), the relationship of the diffraction-point position and the sinusoid of the diffraction angle is linear. In the modern optical microscopes, a series of lenses are combined to make a complex objective so that the linear approximation can be preserved out to large angles (up to the angular semi-aperture of the objective).

Subsequently, for the formation of the image of a sample, as a microscope is generally used for, the light waves converging at the back focal plane of the objective continue so that they all overlap again in the intermediate image plane. There they form a complicated interference pattern—the direct space image of the sample. In this process, the diffraction spots behave like a set of point sources and the image is their diffraction pattern. Thus, it is a double process of Fraunhofer diffraction for a lens to form a magnified image of the object. Mathematically the objective performs a double Fourier transform.<sup>37</sup>

**3.1.2. Diffraction pattern analysis.** As illustrated in Fig. 1, the microporous film forms a very nice, spot diffraction pattern with sixfold symmetry, indicative of the underlying hexagonal order of the micropore array. The average spacing of the pores can be calculated from the diffraction pattern by two-dimensional

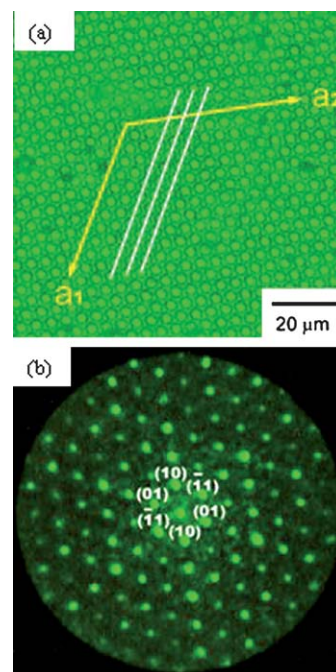


**Fig. 1** Direct-space image (a) and its diffraction pattern (b) of a polystyrene film, cast from a carbon disulfide solution ( $\sim 1\%$  by weight). Imaged by LEICA DMRX microscope with a 40 $\times$  dry objective (NA = 0.75) and an interference filter ( $\lambda = 532 \text{ nm}$ ). Miller indices ( $hk$ ) of the first ring of diffraction spots are shown in (b) with the unit vector direction given in (a). The parallel white lines passing through the center of the air bubbles in (a) are the virtual lattice lines analogous to the parallel planes in a crystal.

Bragg's law, also called grating equation. The detailed discussion of diffraction patterns formed by ordered and randomly arranged particles can be found in any standard text on optical physics,<sup>28,37</sup> and we limit our discussion to diffraction by highly ordered films.

Bragg's law for transmission through a two-dimensional lattice is

$$m\lambda = nd_{hk}\sin\theta, \quad (1)$$

where  $m$  is the order of the diffraction maximum ( $m = 0, 1, 2, \dots$ ),  $\lambda$  is the wavelength of the incident light,  $n$  is the refractive index of the dispersion medium,  $d_{hk}$  is the lattice spacing and  $\theta$  is the angle between the incident and diffracted beams.

For a layer of closely packed spheres,  $d_{hk}$  is the spacing between a set of parallel lines through the centers of the spheres (Fig. 1a), where  $(hk)$  is the two-index specification of a set of parallel lines, analogous to the Miller indices of a set of parallel planes in a crystal.<sup>38,39</sup> The unit cell relationship is

$$d_{hk} = \frac{D}{2} \left[ \frac{3}{h^2 + hk + k^2} \right]^{1/2} \quad (2)$$

where  $D$  is the center-to-center distance of the spheres.<sup>38,39</sup>

In our experiment,  $\lambda$  is 532 nm and the dispersion medium is air so that  $n = n_{\text{air}} = 1$ . Thus, by knowing the angle  $\theta$ , the lattice spacing  $d$  and the center-to-center distance  $D$  can be calculated from eqn (1) and (2). As discussed above, for a microscope objective

$$\sin\theta \propto r_q \quad (3)$$

where  $r_q$  is the distance between the zero<sup>th</sup>-order diffraction spot and the  $m^{\text{th}}$ -order one, which can be directly measured from the diffraction pattern by an image analysis software. Thus, by using a reference with known direct-space spacing ( $d$  or  $D$ ), *e.g.*, an optical grating, the diffraction space, *i.e.*, the reciprocal space, can be calibrated and the values of  $d$  and  $D$  of unknown samples can be calculated from their diffraction patterns.

Here, we use the numerical aperture (NA) of the objective to do the calculation, which makes the calculation rather straightforward. NA is defined as  $n\sin\theta_{\text{NA}}$ , where  $n$  is the refractive index

of the dispersion medium and  $\theta_{\text{NA}}$  is the angular semi-aperture of the objective, *i.e.*, the maximum angle with respect to the optical axis at which diffracted light can be collected by the objective. Diffraction angle  $\theta_{\text{NA}}$  corresponds to the most outside circle in the diffraction pattern (Fig. 1b), thus its sinusoid is proportional to the radius of the NA circle in the diffraction pattern. The values of  $D$  calculated from the spot diffraction pattern for a film (Fig. 1b) are given in Table 1. It is evident from the data that the values calculated from the diffraction pattern compare very favorably with those measured directly from the direct-space image.

While our motivation here is primarily to illustrate how the order seen in real space images can be described and quantified by diffraction analysis commonly applied in crystallography, we can make generic observations about the interaction of light with holey films. Diffraction patterns formed by ordered structures are quite abundant in nature, and provide the gemstone opals as well as certain beetles and snakes with their beautiful colors.<sup>40–42</sup> The possibility of forming porous structures that can be filled with another fluid provides us with a method for producing the “play of color” seen in opals. While the holey films formed with polymers here do show interference colors, increasing the refractive index contrast by incorporating inorganic materials is likely to provide the optical properties required in designing the structures useful in areas ranging from low and high reflection coatings on lenses and mirrors to textured paints with structural color, to just name a few.

## 3.2. Real space analysis of the holey films

**3.2.1. Voronoi polygon analysis of the holey films.** A way to qualitatively check the sixfold order is to look at the coordination number ( $z$ ) of every pore and the fraction ( $P_z$ ) of the pores that exhibit a given coordination  $z$ .<sup>19–21,43</sup> The coordination number ( $z$ ) of a pore is the number of its nearest neighbors. For a perfect hexagonal lattice, all the pores should have six neighbors and  $P_6$  should be one.

In order to determine which pores are neighbors, we use a method based on Voronoi polygons. The Voronoi cell (or Dirichlet region) is the smallest convex polygon surrounding a point, whose sides are perpendicular bisectors of lines between

**Table 1** Center-to-center distance of air bubbles calculated from the diffraction pattern ( $D_{\text{cal}}$ ) according to eqn (1)–(3), comparable with  $D_{\text{meas}} = 4.76$   $\mu\text{m}$  measured from the corresponding direct-space image shown in Fig. 1a

Family of lines	Indices ( $hk$ )	Order ( $m$ )	Average $d_{\text{cal}}/\mu\text{m}$	Average $D_{\text{cal}}/\mu\text{m}$
{10}	(10), (01), ( $\bar{1}1$ )	1	4.09	4.72
		2	4.10	4.74
		3	4.12	4.76
		4	4.09	4.73
		5	4.12	4.75
{11}	(11), ( $\bar{1}2$ ), ( $\bar{2}1$ )	1	2.38	4.75
		2	2.36	4.72
		3	2.37	4.74
{12}	(12), (21), ( $\bar{1}3$ ), ( $\bar{3}1$ ), ( $\bar{2}3$ ), ( $\bar{3}2$ )	1	1.55	4.74
		2	1.55	4.74
{13}	(13), (31), ( $\bar{1}4$ ), ( $\bar{4}1$ ), ( $\bar{3}4$ ), ( $\bar{4}3$ )	1	1.14	4.75
{23}	(23), (32), ( $\bar{2}5$ ), ( $\bar{5}2$ ), ( $\bar{3}5$ ), ( $\bar{5}3$ )	1	0.94	4.74
{14}	(14), (41), (15), (51), (45), (54)	1	0.90	4.74
{15}	(15), (51), ( $\bar{1}6$ ), (61), ( $\bar{5}6$ ), (65)	1	0.74	4.76

the point and its neighbors. While the Voronoi diagram consists of polygons that represent the region closest to the point, it allows one to construct Delaunay (or Delone) tessellation, where non-overlapping simplexes (say triangles on a plane) tessellate the space, providing the necessary toolbox for pattern recognition and for modeling the properties of spatial structures.<sup>44</sup> Two points are said to be neighbors if their respective Voronoi polygons have one side in common.<sup>19,43</sup>

In Fig. 2, two microporous films are shown with their microscopic images and Voronoi polygon analysis. For clarity, only polygons with non-six sides are drawn. Further, the degree of order in a system can be described in terms of the entropy of conformation, defined as  $S = -\sum P_z \ln P_z$ .<sup>19,21,43</sup> The smaller the value of  $S$  is, the higher the degree of order is. We can see, in these films, most polygons are six-sided ( $P_6$  is larger than 0.9), while only a small number of polygons have five and seven sides, other polygons are almost nonexistent.

**3.2.2. Orientational correlation function of the holey films.** To further quantitatively characterize the degree of the order of the hexagonally structured microporous films, we used the bond-orientational correlation function,  $G_6(r)$ . It was first suggested for a two-dimensional melting theory by Nelson and Rubinstein *et al.*,<sup>45</sup> and has been successfully used to identify the ordering and disordering of colloids<sup>29,30,46,47</sup> as well as plasma crystals,<sup>32</sup> liquid crystals<sup>48</sup> and block copolymer assemblies.<sup>33</sup> The “bond” is defined as the imaginary line joining a sphere at  $r = (x, y)$  to its near neighbors (Fig. 3), where the point  $r$  is the projection of the sphere center onto the plane on which it rests.<sup>45</sup> The  $G_6(r)$  measures orientational order of a hexagonal lattice.

The normalized measure of orientational correlation is given by:<sup>45</sup>

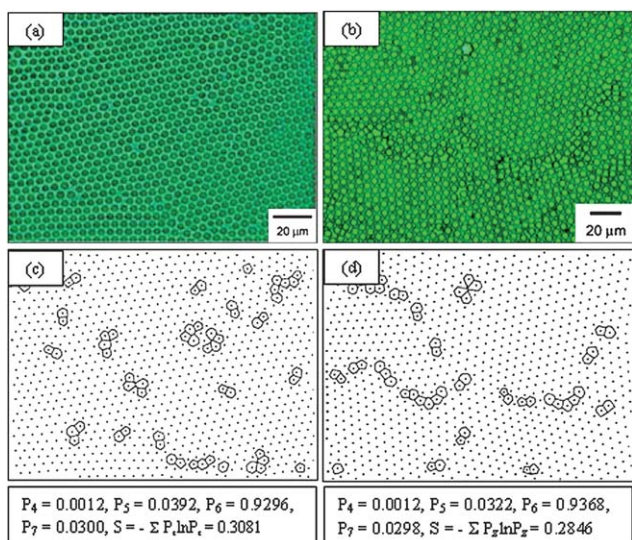


**Fig. 2** Voronoi polygon analysis of hexagonally ordered films. (a) and (b) are optical images of microporous a-PS films, in reflection mode and transmission mode, respectively. (c) and (d) are the correspondent Voronoi polygon analysis of (a) and (b), where the dots correspond to the center of the pores and only polygons with non-six sides are marked. Textboxes below (c) and (d) give the calculated values of the fraction of coordination number ( $P_z$ ) and the entropy of the systems ( $S$ ).

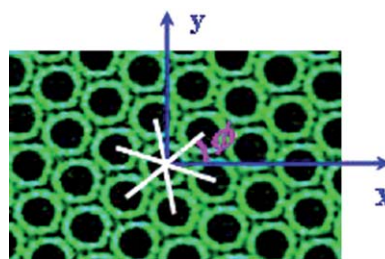


**Fig. 3** The bonds joining a sphere at  $r = (x, y)$  to its near neighbors are shown as white short lines in the image.  $\phi$  is the bond angle with respect to an axis, e.g.,  $x$ -axis here.

$$G_6(r) \equiv \langle \psi_6^*(r) \psi_6^*(0) \rangle / G_b(r) \quad (4)$$

where  $\psi_6(r)$  is the bond-orientational order parameter,

$$\psi_6(r) \equiv \sum_{r_{jk}} \delta(r - r_{jk}) \exp(6i\phi_{jk}) \quad (5)$$

The sum runs over nearest-neighbor bonds centered at  $r_{jk}$  and inclined at an angle  $\phi_{jk}$  with respect to the  $x$ -axis.  $G_b(r)$  represents auto-correlations of bond densities  $\rho_b$ ,

$$\rho_b(r) \equiv \sum_{r_{ij}} \delta(r - r_{ij}) \quad (6)$$

The brackets in eqn (4) represent an average over particle positions and orientations consistent with a separation vector of magnitude  $r$ . It is divided by  $G_b(r)$  to ensure that the correlations do not decay when all bonds carry identical order parameters. For a perfect hexagonal crystal,  $G_6(r)$  would be fixed at unity for all  $r$ . For less ordered hexagonal close-packed solids,  $G_6(r)$  decays with increasing  $r$ . Here, we use the method described by Quinn *et al.*<sup>32</sup> to do the calculations. First the positions of the pore centers are recorded, and then the midpoints  $r_i$  and the angles  $\phi_i$  (with respect to an arbitrary axis) of the bonds which join the pores to their nearest neighbors are calculated. Next a numerical average of  $\cos[6(\phi_i - \phi_0)]$  is performed for all bonds  $i$  whose midpoints are  $r = |r_i - r_0|$  away from the midpoint  $r_0$  of the center bond 0, which has a bond angle  $\phi_0$ . This result is averaged again using each bond as a center bond, yielding  $G_6(r)$ . Some calculated results are shown in Fig. 4.

Comparing the direct space characterization data of the sample films (a) and (b) in Fig. 2, we can see that film 2(a) has a larger value of  $G_6(r)$  (more ordered), but smaller  $P_6$  and larger entropy  $S$  (less ordered) than film 2(b). This is plausible because  $G_6(r)$  measures the long-range orientational order. The orientation of packed pores changes a lot across the grain boundaries in 2(b), thus the  $G_6(r)$  decays faster with distance  $r$ . Meanwhile, for film 2(a), the pore size is not as uniform as that in film 2(b), with some larger or smaller pores locally trapped, leading to more polygons with the number of sides differing from six. However, the long-range orientation of the array of the pores in film 2(a) does not change as much as that in film 2(b).

### 3.3. Real space analysis of assembling water drops

**3.3.1. Voronoi analysis of assembling droplets.** The breath-figure-templated assembly of holey films involves the

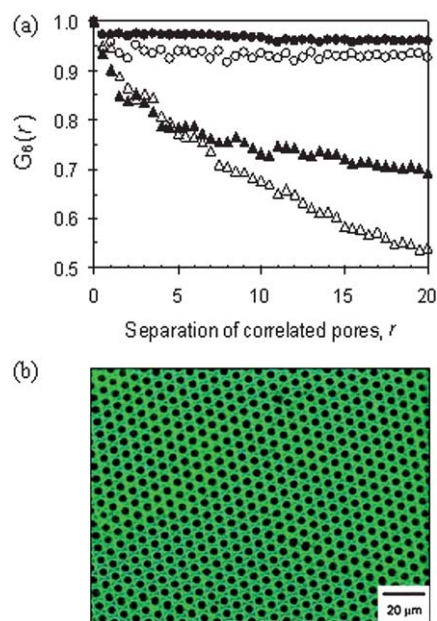


**Fig. 4** (a) Plots of orientational correlation function,  $G_6(r)$ , in units of average spacing of pores, for the samples shown in Fig. 1(a) (○), 2(a) (▲), 2(b) (△), and 4(b) (●), respectively.

crystallization of non-coalescent water drops, followed by subsequent evaporation of water, leaving a porous film. The array of growing water droplets, which appear over evaporating organic liquids or polymer solutions, progressively transform into a highly ordered, hexagonal assembly in two dimensions and in certain cases, form a three-dimensional crystal of non-coalescent water drops. The development of ordered structure from initially randomly distributed drops or clusters of drops is easily observed under a microscope, as shown in Fig. 5.

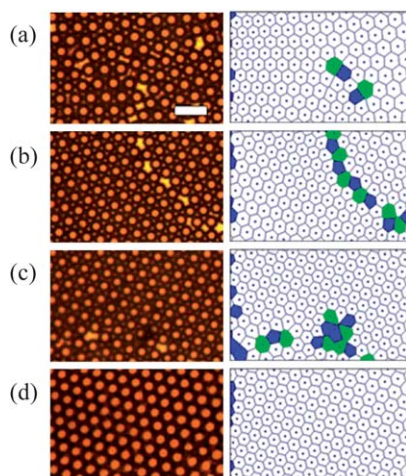


**Fig. 5** Optical images of water droplets growing and packing over hexo-PPE in  $\text{CS}_2$  solution (left) and their Voronoi diagrams (right). Evolution of hexagonally packed array of water droplets is accompanied by corresponding increase in the number of hexagons (and hence the decrease in pentagons/heptagons) in the Voronoi analysis. Pentagons are dark gray (blue online), while heptagons are light gray (green online). Each successive image from (a) to (d) is 4 s apart.

Curiously, the water droplets behave like atoms or colloidal particles<sup>49</sup> or bubble rafts,<sup>50,51</sup> and produce a range of defects and dislocations associated with two-dimensional crystals.<sup>52,53</sup> These include vacancies, defects due to the presence of foreign atoms, stacking faults and grain boundaries. The physics that governs the nucleation, growth, non-coalescence and assembly of water drops is described and discussed elsewhere.<sup>52,53</sup> In this paper, we limit the discussion to the characterization of local arrangement of drops as revealed by using a Voronoi construction as shown in Fig. 5. Also, the presence of drops that are surrounded by five or seven drops is illustrated by colored/filled cells, and the increase in order is reflected in increase in the number of hexagonal cells as shown in Fig. 5. Notice that the pentagons and heptagons typically occur as a pair, or form a chain. The chain is seen to form at the place where grain boundary occurs. The grain boundaries and stacking defects are progressively removed as water drops pack into a highly ordered structure, as seen in the last image of the panel. It is worth pointing out that a highly ordered array of pores is obtained after these water drops evaporate away, only when the pattern formed by water drops itself shows a high degree of order. We must remark, however, that the Voronoi analysis of hexatic phase formed by drops condensed over pre-cooled passive liquids shows a much higher degree of disorder:<sup>54</sup> the number of hexagons is lower and most polygons are of different sizes, revealing larger heterogeneity in both the size of drops and the distance between drops. The dynamics of pairs of pentagonal and heptagonal polygons, called penta–hepta domains (PHDs), has been studied before in the Bernard–Marangoni systems (non-equilibrium system)<sup>35,36</sup> as well as ordering of soap bubbles<sup>31</sup> (equilibrium assembly). In either case, the defects tend to disappear over time, indicating that the system tries to select ordered hexagonal pattern preferentially, as it is likely to be the system with minimum free energy for a two dimensional assembly where curvature effects are not relevant.<sup>55</sup>

Indeed, the presence of five and seven sided polygons existing in the first three Voronoi images in Fig. 5, or in Fig. 2, could arise from either curvature effects or from stacking faults in a planar two dimensional assembly.<sup>55</sup> As the final structure (last image in Fig. 5) has no pentagons or heptagons, the series of images show stacking faults only. It is well known that a curved surface like buckyballs cannot be tessellated by hexagons only, and at least a dozen pentagons are required to account for curvature.<sup>56</sup> A higher number of pentagons and additional heptagons are found on curved substrates as seen in the Voronoi analysis of bubble rafts,<sup>57</sup> colloidosomes<sup>58</sup> or in patterns found on the exoskeleton of an iridescent jewel beetle called *Chrysinia Gloriosa*.<sup>59</sup> A higher number of pentagons and heptagons arise in these systems, as according to Nelson,<sup>56</sup> systems with large  $R/a$  can minimize the free energy by incorporating additional grain boundaries.<sup>56</sup> Here  $R$  refers to the curvature and  $a$  to the size of colloid, bubble, or particle relevant to the system (equal to droplet radius). While it will be interesting to see such stacking faults in a breath-figure-templated pattern formed on curved surface, in the examples discussed in this paper, the process was carried out on flat substrates only. In any case, when the surface is curved, only a limited region on substrate appears to be in focus on the microscope, and in the examples included here, no curvature is visible at least up to 1000 drop diameters, from the drops or

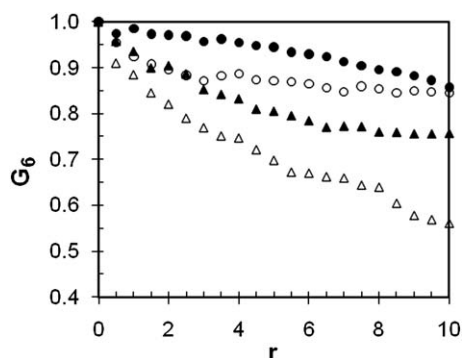


**Fig. 6** Plots of orientational correlation function,  $G_6(r)$ , in units of average spacing of pores, for the four images shown in Fig. 5: (a)  $\Delta$ , (b)  $\blacktriangle$ , (c)  $\circ$ , and (d)  $\bullet$ .

pores captured in figures included herewith. The ordered microstructured PPE films (conjugated, semiconducting polymer) show a high degree of order, and were described at length in a previous publication.<sup>9</sup>

**3.3.2. Orientational correlation function of assembling droplets.** In an earlier sub-section, we described the degree of the order of the hexagonally structured microporous films can be represented by bond-orientational correlation function,  $G_6(r)$ . The increase in order observed in Fig. 5 can be quantified in terms of  $G_6(r)$  as well, and Fig. 6 shows how the increase in order leads to higher bond-orientation correlation, extending up to  $10r$ , where  $r$  is the distance from a central drop expressed in units of  $a$ , that is the size of water drop. The bond-orientation correlation functions shown in Fig. 6 correspond to the four images shown in Fig. 5 and where open triangles show the lower value of order in the first frame while filled circles show how increase in order leads to stronger bond correlations for larger distances. The presence of highest order in last image is brought about by the rearrangement of water drops that seek to maximize their packing efficiency by organizing themselves into a highly ordered structure.

## 4. Conclusions

We have examined and characterized the two-dimensional closely packed array of pores in a polymer film, *via* diffraction pattern analysis, orientational correlation function, and Voronoi polygon analysis (coordination and entropy). For the films forming at different conditions or the images of one film at different formation stages, it is helpful to characterize the order for better understanding of the mechanism of the formation of the order structure in the film. The present study illustrates how the degree of order present in assembling arrays of water drops grows over time. The use of optical microscope for diffraction pattern analysis allows quantitative comparison between different polymer film. Further the well-established principles of crystallography can be applied to understand and describe the microstructured films. Contrastingly, the analysis of patterns in real space using a combination of Voronoi analysis and orientational correlation function allows us to look at short range and long range order, respectively.

## Acknowledgements

This work was partially supported by the NSF funding (DMR-0603026) for MS and JOP. The authors would like to thank Prof. Uwe Bunz for his generous donation of hexo-PPE. MS also acknowledges support from WCU (World Class University) program through the National Research Foundation of Korea funded by the Ministry of Education, Science and Technology (R32-2008-000-10142-0). Both LS and VS carried major part of this research as graduate students in Georgia Institute of Technology.

## References

- G. Widawski, M. Rawiso and B. Francois, *Nature*, 1994, **369**, 387–389.
- M. Srinivasarao, D. Collings, A. Philips and S. Patel, *Science*, 2001, **292**, 79–83.
- O. Karthaus, N. Maruyama, X. Cieren, M. Shimomura, H. Hasegawa and T. Hashimoto, *Langmuir*, 2000, **16**, 6071–6076.
- O. Pitois and B. Francois, *Eur. Phys. J. B*, 1999, **8**, 225–231.
- S. S. Sheiko, A. Mourran and M. Moller, *Abstr. Pap. Am. Chem. Soc.*, 1999, **218**, PMSE, U610-U610.
- M. H. Stenzel, *Aust. J. Chem.*, 2002, **55**, 239–243.
- B. de Boer, U. Stalmach, H. Nijland and G. Hadziioannou, *Adv. Mater.*, 2000, **12**, 1581–1583.
- M. H. Stenzel-Rosenbaum, T. P. Davis, A. G. Fane and V. Chen, *Angew. Chem., Int. Ed.*, 2001, **40**, 3428–3432.
- L. Song, R. K. Bly, J. N. Wilson, S. Bakkab, J. O. Park, M. Srinivasarao and U. H. F. Bunz, *Adv. Mater.*, 2004, **16**, 115–118.
- B. Erdogan, L. L. Song, J. N. Wilson, J. O. Park, M. Srinivasarao and U. H. F. Bunz, *J. Am. Chem. Soc.*, 2004, **126**, 3678–3679.
- T. Nishikawa, J. Nishida, R. Ookura, S. I. Nishimura, S. Wada, T. Karino and M. Shimomura, *Mater. Sci. Eng., C*, 1999, **8–9**, 495–500.
- T. Nishikawa, M. Nonomura, K. Arai, J. Hayashi, T. Sawadaishi, Y. Nishiura, M. Hara and M. Shimomura, *Langmuir*, 2003, **19**, 6193–6201.
- M. S. Barrow, R. L. Jones, J. O. Park, C. J. Wright, P. R. Williams and M. Srinivasarao, *Mod. Phys. Lett. B*, 2008, **22**, 1989–1996.
- V. Sharma, L. Song, R. L. Jones, M. S. Barrow, P. R. Williams and M. Srinivasarao, *Europhys. Lett.*, 2010, **91**, 38001–38006.
- L. Rayleigh, *Nature*, 1911, **86**, 416–418.
- D. Beysens, A. Steyer, P. Guenoun, D. Fritter and C. M. Knobler, *Phase Transitions*, 1991, **31**, 219–246.
- F. Family and P. Meakin, *Phys. Rev. Lett.*, 1988, **61**, 428–431.
- B. J. Briscoe and K. P. Galvin, *J. Phys. D: Appl. Phys.*, 1990, **23**, 422–428.
- A. Steyer, P. Guenoun, D. Beysens and C. M. Knobler, *Phys. Rev. B: Condens. Matter Mater. Phys.*, 1990, **42**, 1086–1089.
- A. Steyer, P. Guenoun and D. Beysens, *Phys. Rev. E: Stat. Phys., Plasmas, Fluids, Relat. Interdiscip. Top.*, 1993, **48**, 428–431.
- A. V. Limaye, R. D. Narhe, A. M. Dhote and S. B. Ogale, *Phys. Rev. Lett.*, 1996, **76**, 3762–3765.
- N. Wakamatsu, H. Takamori, T. Fujigaya and N. Nakashima, *Adv. Funct. Mater.*, 2009, **19**, 311–316.
- S. H. Lee, J. S. Park, B. K. Lim, C. Bin Mo, W. J. Lee, J. M. Lee, S. H. Hong and S. O. Kim, *Soft Matter*, 2009, **5**, 2343–2346.
- B. C. Englert, S. Scholz, P. L. Leech, M. Srinivasarao and U. H. F. Bunz, *Chem.–Eur. J.*, 2005, **11**, 995–1000.
- M. Pintani, J. Huang, M. C. Ramon and D. D. C. Bradley, *J. Phys.: Condens. Matter*, 2007, **19**, 016203, 1–9.
- M. H. Nurmawati, R. Renu, P. K. Ajikumar, S. Sindhu, F. C. Cheong, C. H. Sow and S. Valiyaveetil, *Adv. Funct. Mater.*, 2006, **16**, 2340–2345.
- Y. Zhang and C. Wang, *Adv. Mater.*, 2007, **19**, 913–916.
- A. Sommerfeld, *Optics: Lectures on Theoretical Physics*, Academic Press, New York, 1954, vol. 4.
- C. A. Murray, W. O. Sprenger and R. A. Wenk, *Phys. Rev. B: Condens. Matter Mater. Phys.*, 1990, **42**, 688–703.
- D. G. Grier and C. A. Murray, *J. Chem. Phys.*, 1994, **100**, 9088–9095.

- 31 T. Tam, D. Ohata and M. M. Wu, *Phys. Rev. E: Stat. Phys., Plasmas, Fluids, Relat. Interdiscip. Top.*, 2000, **61**, R9–R12.
- 32 R. A. Quinn, C. Cui, J. Goree, J. B. Pieper, H. Thomas and G. E. Morfill, *Phys. Rev. E: Stat. Phys., Plasmas, Fluids, Relat. Interdiscip. Top.*, 1996, **53**, R2049–R2052.
- 33 R. A. Segalman, A. Hexemer, R. C. Hayward and E. J. Kramer, *Macromolecules*, 2003, **36**, 3272–3288.
- 34 P. Cerisier, R. Occelli, C. Perezgarcia and C. Jamond, *J. Phys. (Paris)*, 1987, **48**, 569–576.
- 35 D. Semwogerere and M. F. Schatz, *Phys. Rev. Lett.*, 2002, **88**, 4.
- 36 L. S. Tsimring, *Phys. Rev. Lett.*, 1995, **74**, 4201–4204.
- 37 S. G. Lipson, H. Lipson and D. S. Tannhauser, *Optical Physics*, Cambridge University Press, Cambridge, 1995.
- 38 A. S. Nowick and S. R. Mader, *IBM J. Res. Dev.*, 1965, **9**, 358–374.
- 39 J. W. Goodwin, R. H. Ottewill and A. Parentich, *J. Phys. Chem.*, 1980, **84**, 1580–1586.
- 40 M. Srinivasarao, *Chem. Rev.*, 1999, **99**, 1935–1961.
- 41 A. R. Parker, *J. Opt. A: Pure Appl. Opt.*, 2000, **2**, R15–R28.
- 42 K. Nassau, *The Physics and Chemistry of Color*, John Wiley & Sons, Inc., New York, 2001.
- 43 D. Weaire and N. Rivier, *Contemp. Phys.*, 1984, **25**, 59–99.
- 44 A. Okabe, B. Boots, K. Sugihara and S. N. Chiu, *Spatial Tessellations: Concepts and Applications of Voronoi Diagrams*, John Wiley & sons, Inc., New York, 2000.
- 45 D. R. Nelson, M. Rubinstein and F. Spaepen, *Philos. Mag. A*, 1982, **46**, 105–126.
- 46 B. I. Halperin and D. R. Nelson, *Phys. Rev. Lett.*, 1978, **41**, 121–124.
- 47 D. R. Nelson, *Phys. Rev. B: Condens. Matter Mater. Phys.*, 1983, **28**, 5515–5535.
- 48 R. Bruinsma and D. R. Nelson, *Phys. Rev. B: Condens. Matter Mater. Phys.*, 1981, **23**, 402–410.
- 49 P. Pieranski, *Contemp. Phys.*, 1983, **24**, 25–73.
- 50 L. Bragg and W. M. Lomer, *Proc. R. Soc. London, Ser. A*, 1949, **196**, 171–181.
- 51 L. Bragg and J. F. Nye, *Proc. R. Soc. London, Ser. A*, 1947, **190**, 474.
- 52 V. Sharma, PhD thesis, Georgia Institute of Technology, 2008.
- 53 V. Sharma, L. Song and M. Srinivasarao, in preparation.
- 54 A. Steyer, P. Guenoun, D. Beysens and C. M. Knobler, *Phys. Rev. B: Condens. Matter Mater. Phys.*, 1990, **42**, 1086–1089.
- 55 M. J. Bowick and L. Giomi, *Adv. Phys.*, 2009, **58**, 449–563.
- 56 D. R. Nelson, *Spherical Crystallography: Virus Buckling and Grain Boundary Scars*, 2004.
- 57 M. J. Bowick, L. Giomi, H. Shin and C. K. Thomas, *Phys. Rev. E: Stat., Nonlinear, Soft Matter Phys.*, 2008, **77**, 021602, 1–5.
- 58 A. D. Dinsmore, M. F. Hsu, M. G. Nikolaides, M. Marquez, A. R. Bausch and D. A. Weitz, *Science*, 2002, **298**, 1006–1009.
- 59 V. Sharma, M. Crne, J. O. Park and M. Srinivasarao, *Science*, 2009, **325**, 449–451.